DOI 10.5162/sensor2017/B6.2

Incoherent Optical Frequency Domain Reflectometry for Distributed Raman and Bragg Fiber Temperature Sensors

Max Köppel[1], Stefan Werzinger[1], Rainer Engelbrecht[2], Jan-Robert Sutter[1], Sven Bergdolt[1], and Bernhard Schmauss[1]
[1] Institute of Microwaves and Photonics, Friedrich-Alexander University Erlangen-Nürnberg (FAU), Cauerstr. 9, 91058 Erlangen, Germany,
[2] Polymer Optical Fiber Application Center (POF-AC), University of Applied Sciences Georg-Simon-Ohm Nürnberg, Wassertorstr. 10, 90489 Nürnberg, Germany
max.koeppel@fau.de

Abstract:
Optical temperature sensors have become indispensable for many important future technologies, for example in the energy sector. However, most commercially available systems offer either distributed measurements or high temperature resolution at distinct hot spots since they are restricted to one measurement principle. We have combined two concepts, fiber Bragg grating (FBG) temperature sensors and Raman based distributed temperature sensing, to overcome these limitations. Our incoherent optical frequency domain reflectometry (IOFDR) system allows to perform truly distributed temperature measurements with a mean standard deviation of 1.5 K at a spatial resolution in the order of 1 m and FBG hot spot measurements using a single measurement setup.

Key words: Optical temperature sensor, Raman DTS, distributed sensing, FBG temperature sensor, incoherent optical frequency domain reflectometry

Fiber Optical Temperature Sensing

An important application for fiber sensors is temperature monitoring. One of the main advantages of fiber sensors is that long distances can be covered and that the sensor fibers are insensitive to electromagnetic fields. This allows to deploy fiber optic sensors in all kinds of industrial environments and energy facilities [1]. Several sensors can be cascaded or multiplexed to measure at a series of distant locations using only a single, centrally installed measurement unit, which reduces costs and complexity.

There are various different measurement concepts that are either based on temperature depended scattering phenomena (Rayleigh, Brillouin, Raman scattering) [2] or deploy distinct temperature sensitive fiber components such as fiber Bragg gratings (FBGs) [3].

While scattering based concepts enable truly distributed temperature sensing (DTS), FBG sensors are better suited for the monitoring of hot spots at distinct positions with a good temperature resolution.

In order to profit from the advantages of both concepts we have combined a Raman-based DTS with FBG temperature sensors in one measurement setup using incoherent optical frequency domain reflectometry (IOFDR).

Spatially Resolved Backscatter and Reflection Measurements with Incoherent Optical Frequency Domain Reflectometry

For both concepts, a method to spatially resolve the backscattered and reflected light along the fiber is needed. In a Raman DTS system, the temperature measurement is based on the power ratio of the Raman Stokes and anti-Stokes backscattering components, whereas for the FBG sensors the spatial resolution, in addition to the wavelength resolution, is crucial to separate the individual FBG sensors.

Conventional optical time domain reflectometry (OTDR) systems launch an optical pulse into the fiber and measure the backscattered and reflected light over time. This so-called impulse response $h_{\mathrm{F}}(t)$ can be related to spatial fiber coordinates via the group velocity of light in the fiber, resulting in a backscattering/reflection profile $R(z)$.

However, the same information can be obtained by measuring the frequency response $H_{\mathrm{F}}(f)$ of the sensor fiber and calculating $h_{\mathrm{F}}(t)$ via the inverse Fourier transform (IFT). This approach is

called IOFDR and offers various advantages over OTDR, such as lower peak-to-average power and accurate calibration capabilities.

Experimental IOFDR System Setup

In order to measure the frequency response $H_{\mathrm{F}}(f)$ of a sensor fiber, a spectrally broadened continuous-wave light source is intensity-modulated with frequencies up to some hundred MHz with the stimulus signal of a vector network analyzer (VNA). The light, which is back propagating along the fiber, is separated with a circulator, spectrally split up in an optical filter bank and each component is detected with a fast photodiode. The VNA determines the amplitude and phase of the detected signals relative to the stimulus signal (see Fig. 1).

Measuring at many uniformly spaced frequencies and normalizing to a reference trace gives the discrete frequency response $H_{\mathrm{F}}(f)$ of the sensor fiber. Calculating an IFT yields the corresponding impulse response $h_{\mathrm{F}}(t)$ in the time domain. The limited electrical measurement bandwidth resembles a rectangular window, resulting in a sinc-shaped reconstruction kernel [4]. Optionally, another window function can be multiplied to the measured frequency response before the transformation into the time domain.

From the backscatter impulse response $h_{\mathrm{F}}(t)$ the backscattering profile $R(z)$ is obtained by estimating the DC component and rescaling the abscissa using

$$z(t) = \frac{1}{2} v_{\mathrm{g}} t, \tag{1}$$

where v_{g} is the effective group velocity in the sensor fiber. The DC component corresponds to an up-shift of the backscattering profile and cannot be measured directly with the VNA. However, it can be accounted for by subtracting the noise floor offset after the end of the fiber.

The nominal achievable spatial resolution Δz for this approach is given by [5]

$$\Delta z = \frac{v_{\mathrm{g}}}{2B}, \tag{2}$$

where B is the electrical measurement bandwidth of the VNA.

This value corresponds to the distance between the first zero crossings of the sinc reconstruction kernel if no window is applied. However, even small reflections, e.g. at fiber connectors, cause side lobe artefacts that must be suppressed with the help of an effective window at the cost of a decreased effective spatial resolution.

The maximum unambiguous measurement range $z_{\max}$ is limited by the number of measurement frequencies N, yielding [5]:

$$z_{\max} = \frac{v_{\mathrm{g}}}{2B} \cdot (N-1) = \frac{v_{\mathrm{g}}}{2\Delta f}, \tag{3}$$

with Δf resembling the frequency step size of the VNA.

Fiber Bragg Grating Temperature Sensing

FBGs are point sensors for temperature measurements and therefore suitable for selective thermal hot spot monitoring. Their periodic refractive index modulation causes a narrowband back reflection at the so-called Bragg wavelength given by the Bragg condition $\lambda_{\mathrm{B}} = 2n_{\mathrm{eff}}\Lambda$, where n_{eff} is the effective refractive index of the fiber and Λ the grating period. Both of these parameters depend on temperature and strain, resulting in a shift of the Bragg wavelength $\Delta\lambda_{\mathrm{B}} = \lambda_{\mathrm{B}} - \lambda_{\mathrm{B0}}$ relative to the wavelength λ_{B0} at a reference temperature T_0 and strain. In order to measure temperature changes $\Delta T = T - T_0$ only, it is necessary that the FBGs are either strain compensated or mechanically decoupled from any strain.

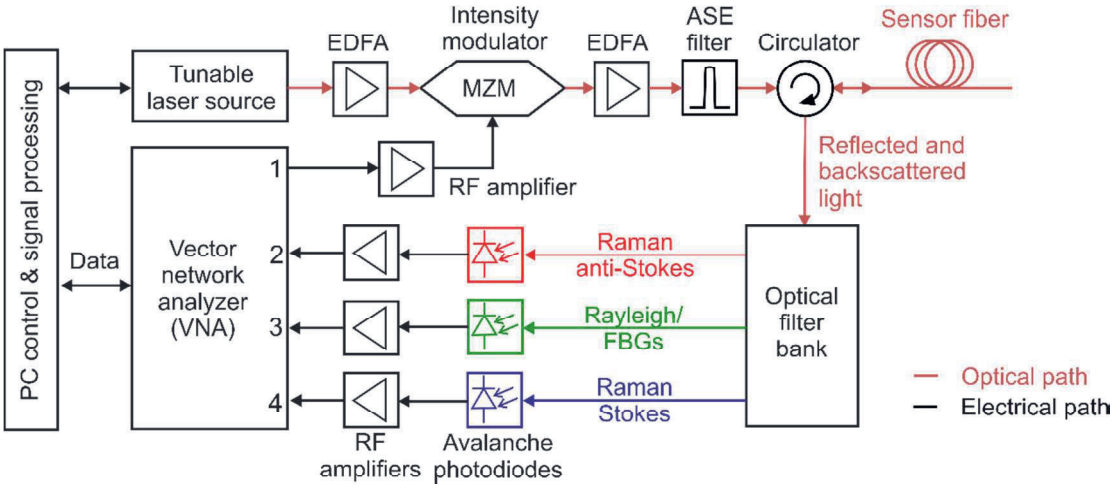

Fig. 1: Experimental IOFDR system setup

Generally, the temperature dependence of the Bragg wavelength follows a nonlinear function [6], which is usually expanded into a Taylor series:

$$\Delta\lambda_{\mathrm{B}}(T) = \frac{\partial\lambda_{\mathrm{B}}}{\partial T}\Delta T + \frac{1}{2}\frac{\partial^2\lambda_{\mathrm{B}}}{\partial T^2}\Delta T^2 + \cdots. \qquad (4)$$

In many applications, the linear temperature coefficient $\frac{\partial\lambda_{\mathrm{B}}}{\partial T}$ is sufficiently accurate. However, for wide temperature ranges and better accuracy, higher order terms should be taken into account in the calibration process.

The Bragg wavelength of a FBG sensor is determined by examining the reflectivity during a wavelength scan of a tunable laser source (TLS) [7]. A set of several FBGs with the same or similar Bragg wavelengths can be separated spatially by performing IOFDR measurements at each wavelength step.

The spectral signatures of the gratings are reconstructed using a model-based compressed sensing (MBCS) approach [8], where the fixed positions of the FBGs are used as prior knowledge and the reflectivities are estimated from the measured frequency response.

Two FBG arrays, each containing three gratings in a spacing of 2 m, were fabricated and recoated again in a HI1060 FLEX fiber. The first grating array was fabricated without hydrogen loading, reaching reflectivities of ~0.2%, whereas for the second grating array a hydrogen-loaded fiber was used, resulting in reflectivities of ~1%.

Prior to the temperature measurements, a calibration of the Bragg wavelengths over temperature is performed. Therefore, the gratings are installed in a temperature control unit with thermoelectric coolers (TEC) and ten temperature cycles ranging from 0 °C to 80 °C in steps of 10 K are run.

The Bragg wavelengths are determined by a Gaussian fit with a threshold of 20% from the reconstructed reflectivity profiles (see calibration points in Fig. 2). At a temperature of 20 °C, the grating array with lower reflectivities (labelled FBG 1-3) contains one FBG with a Bragg wavelength of 1540.6 nm and two gratings at 1541.3 nm, whereas all FBGs of the second array (labelled FBG 4-6) are centered around 1538.9 nm. These differences are probably due to the hydrogen treatment of the second grating array prior to the fabrication.

Looking closer at the calibration points in Fig. 2, a slightly nonlinear characteristic can be observed towards lower temperatures. Therefore, a second order polynomial was fitted to the calibration data (see Fig. 2).

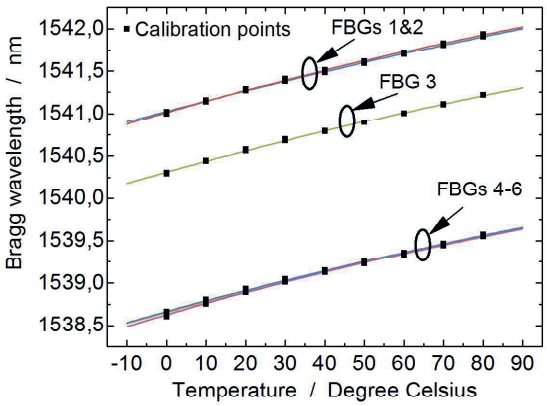

Fig. 2: Calibration curves for the FBGs used in the temperature measurement experiment

The average root mean square error (RMSE) of the calibration curves is approximately 8 pm, which would correspond to a temperature uncertainty of about 0.6 K to 0.7 K for these gratings.

Distributed Raman Temperature Sensing

Raman scattering of light in a fiber causes a Stokes wave and an anti-Stokes wave at wavelengths above and below the pump wavelength that can be observed in the backscattered light. The center frequencies of these components are shifted by the frequency of the molecule vibrations f_{vib} in the fiber. In silica fibers, f_{vib} is about 13 THz [9], leading to a wavelength shift of approx. 100 nm at a pump wavelength λ_0 of 1540 nm. Moreover, a spectral broadening occurs due to the interaction between the molecules in a solid medium. The resulting spectra of the two Raman components can be separated with an optical filter bank. For sensing applications, the dependence of the ratio between the intensity of the anti-Stokes wave $I_{\mathrm{AS},0}$ and the Stokes wave $I_{\mathrm{S},0}$ on the fiber temperature T is exploited [9], [10]:

$$\frac{I_{\mathrm{AS},0}}{I_{\mathrm{S},0}} = \left(\frac{f_{\mathrm{AS}}}{f_{\mathrm{S}}}\right)^4 \cdot \exp\left(-\frac{h \cdot f_{\mathrm{vib}}}{kT}\right). \qquad (5)$$

In Eq. (5), f_{AS} and f_{S} is the frequency of the anti-Stokes and Stokes wave, respectively, h is Planck's constant and k Boltzmann's constant.

For a practical application, Eq. (5) must be extended due to the wavelength dependence of the backscatter capture fraction η in a fiber, and the differences in the detector sensitivity R_{resp}. Neglecting the slightly differing fiber attenuation for the Raman components yields:

$$\frac{I_{\mathrm{AS}}(z)}{I_{\mathrm{S}}(z)} = \frac{R_{\mathrm{resp,AS}}}{R_{\mathrm{resp,S}}} \cdot \frac{\eta_{\mathrm{AS}}}{\eta_{\mathrm{S}}} \cdot \left(\frac{f_{\mathrm{AS}}}{f_{\mathrm{S}}}\right)^4 \cdot \exp\left(-\frac{h \cdot f_{\mathrm{vib}}}{kT}\right). \qquad (6)$$

Filter Bank Setup and Characteristics

The proposed filter bank setup to separate the Raman Stokes, Raman anti-Stokes backscattering and FBG reflections, designed for a pump wavelength of 1540 ± 2 nm, is shown in Fig. 3. A wavelength division multiplexer (WDM) is used at the input to split off the Raman anti-Stokes component, which generally has the lowest power. The spectral Rayleigh/FBG and Raman Stokes content is separated using a free space long-pass edge filter installed after a circulator.

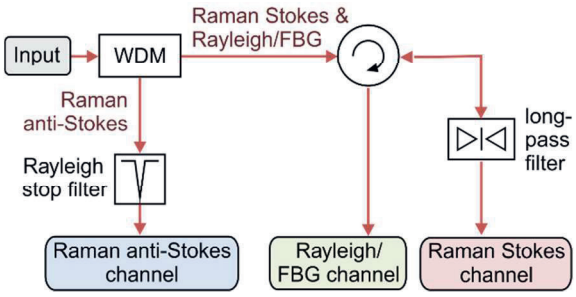

Fig. 3: Setup of the filter bank, that is used to separate the Raman components and the FBG reflections

Fig. 4 shows the transmission characteristic of the filter bank channels. With our setup, a very good isolation between the Rayleigh/FBG channel and the two Raman channels of about 70 dB is achieved. However, there is some extent of crosstalk between the channels. Especially the non-ideal separation of the Raman channels must be considered when the temperature is calculated.

Moreover, the two filter channels will generally experience different attenuations a_{AS} and a_{S}. Therefore, the measured ration of power in the anti-Stokes and Stokes wave can be expressed as:

$$\frac{I'_{\mathrm{AS}}(z)}{I'_{\mathrm{S}}(z)} = \frac{a_{\mathrm{AS}}}{a_{\mathrm{S}}} \cdot \left(\frac{I_{\mathrm{AS}}(z)}{I_{\mathrm{S}}(z)} \cdot \frac{1}{1-x} + \frac{x}{1-x} \right), \qquad (7)$$

where x is the factor of coupling from the Stokes into the anti-Stokes channel. The various factors can be replaced by two calibration coefficients C_1 and C_2, that must be determined in a calibration measurement at a known temperature:

$$\frac{I'_{\mathrm{AS}}(z)}{I'_{\mathrm{S}}(z)} = C_1 \cdot \exp\left(-\frac{h \cdot f_{\mathrm{vib}}}{kT(z)} \right) + C_2. \qquad (8)$$

Rearranging Eq. (8) gives the temperature profile $T(z)$ along the fiber in dependence of the measured, spatially resolved backscattering ratio $I'_{\mathrm{AS}}(z)/I'_{\mathrm{S}}(z)$ at the output of the filter bank:

$$T(z) = -\frac{h \cdot f_{\mathrm{vib}}}{k \cdot \left(\ln\left(\frac{I'_{\mathrm{AS}}(z)}{I'_{\mathrm{S}}(z)} - C_2 \right) - \ln C_1 \right)}. \qquad (9)$$

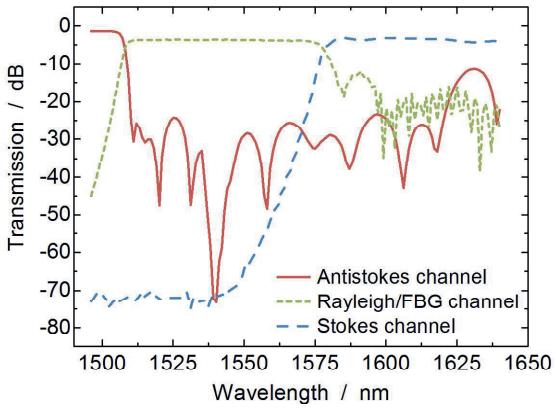

Fig. 4: Transmission characteristic of the proposed filter bank topology

In Fig. 5, the attenuation compensated spectra at the filter bank outputs, measured with an optical spectrum analyzer, are depicted for a 300 m long HI1060 FLEX fiber at three different temperatures. This fiber is especially well suited for a Raman DTS since it exhibits a relatively high amount of Raman scattering [9]. The various backscattering components and the temperature dependence of the Raman anti-Stokes power density is clearly visible.

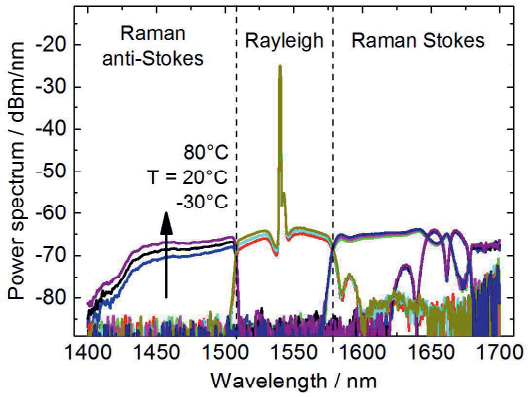

Fig. 5: Measured backscattering spectra at the filter bank outputs for a 300 m HI1060 FLEX fiber (resolution bandwidth: 1 nm)

Experimental Temperature Measurements

For the temperature measurement experiments, we placed a sensor fiber, which consisted of the aforementioned FBG arrays spliced to either end of a 50 m HI1060 FLEX fiber, in the climate chamber at different temperatures. Before and after the sensor fiber, a 50 m lead fiber of the same type was installed (see Fig. 6). At the end of the fiber chain, a short piece of coreless fiber was used as a fiber termination.

Initially, the whole setup was left settled at room temperature and a reference measurement was performed. From the acquired backscattering profile, the connector losses between the fiber segments were determined.

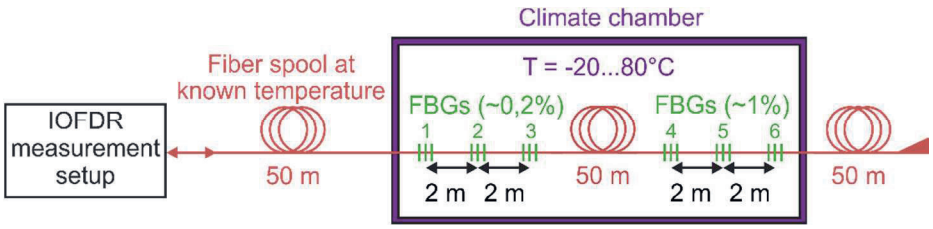

Fig. 6: Fiber setup for the experimental temperature measurements

Subsequently, the climate chamber was set to temperatures ranging from -20 °C to 80 °C in steps of 20 °C. For each temperature step, the TLS performed a wavelength sweep from 1538 nm to 1542.5 nm (step size: 20 pm) and the frequency response of the Rayleigh/FBG channel was measured with the VNA at each wavelength step. From the acquired data set, the spectral shapes of all FBGs were reconstructed (see Fig. 7), the Bragg wavelengths determined and the corresponding temperatures calculated using the calibration curves depicted in Fig. 2.

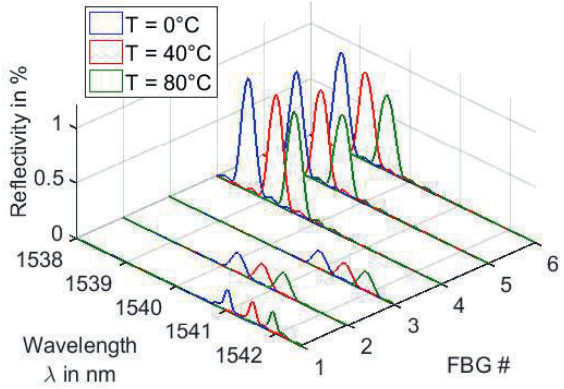

Fig. 7: Examples of reconstructed FBG reflectivities at three different temperatures using MBCS

The Raman measurements were performed at different wavelengths around 1540 nm, where the FBGs showed little reflectivity to minimize their influence. The Raman Stokes and anti-Stokes backscattering profiles along the fiber were reconstructed applying the inverse fast Fourier transform (IFFT) to the frequency response determined at the corresponding filter bank outputs. Before the calculation of the IFFT, a Blackman window function was applied to suppress unwanted side lobes. From the backscattering profiles, the temperature profile was calculated according to Eq. (9).

The room temperature was recorded and the 50 m lead fiber was used to estimate the required calibration coefficients C_1 and C_2 with a least square fit for each measurement.

The measurement parameters of the VNA for the RF sweeps are listed in Tab. 1. For the Raman DTS measurements, these parameters yield a maximum unambiguous measurement range $z_{\max}$ of almost 3.5 km and a spatial resolution Δz of around 1 m. However, due to the Blackman window, the main lobe is broadened by a factor of approximately 2 [4].

For the FBG reconstruction, the MBCS approach [8] was chosen, which allowed using the same modulation bandwidth of only 100 MHz.

For all measurements, the fiber launch power was approximately 26 dBm.

Tab. 1: VNA measurement parameters for the Raman DTS and FBG temperature sensor measurements

VNA Parameter	Raman DTS	FBG sensors
Start Frequency	30 kHz	500 kHz
Stop Frequency	99.99 MHz	100 MHz
IF bandwidth	30 Hz	10 kHz
Number of frequency samples	3,333	200
Averaging	10	-

The results of the FBG and Raman temperature measurements are depicted in Fig. 8. A good agreement was found between the temperatures measured with the FBG sensors and the Raman DTS results.

In the Raman DTS measurements, an average accuracy better than 0.5 K, a worst-case standard deviation of around 2.5 K and a mean deviation of 1.5 K was achieved for the sensor fiber inside the climate chamber.

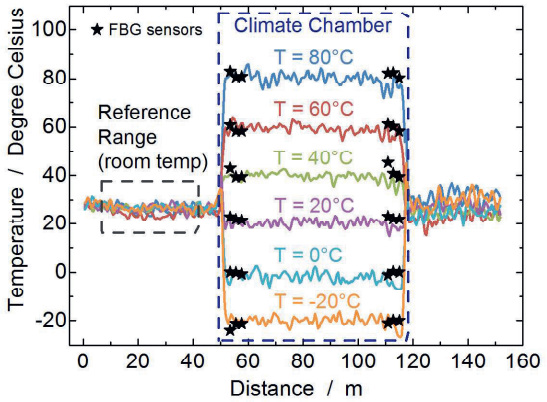

Fig. 8: Temperature measurement results

Summary

In this work, we have successfully demonstrated a fiber optical temperature measurement system based on IOFDR, which combines FBG temperature sensors and Raman based DTS to enable both, distinct hot spot and truly distributed temperature profile measurements with a spatial resolution in the order of 1 m, over a wide range of temperatures.

Acknowledgements

Parts of this work were funded by the German Federal Ministry for Economic Affairs and Energy (BmWE) under the grant no. 03ET7522B (project "iMonet").
We would like to thank the AOS GmbH (Dresden, Germany) for the fabrication of the FBG sensor samples used for the temperature measurement experiment in this work.

References

[1] C. Hu, J. Wang, Z. Zhang, S. Jin, and Y. Jin, Application research of distributed optical fiber temperature sensor in power system*, 2011 Asia Communications and Photonics Conference and Exhibition (ACP)*, Shanghai (2011), pp. 1-6; doi: 10.1117/12.905303

[2] A. Ukil, H. Braendle, and P. Krippner, Distributed Temperature Sensing: Review of Technology and Applications, in *IEEE Sensors Journal*, vol. 12, no. 5, pp. 885-892 (2012); doi: 10.1109/JSEN.2011.2162060

[3] A. D. Kersey *et al*., Fiber grating sensors, in *Journal of Lightwave Technology*, vol. 15, no. 8, pp. 1442-1463 (1997); doi: 10.1109/50.618377

[4] F. J. Harris, On the use of windows for harmonic analysis with the discrete Fourier transform, in *Proceedings of the IEEE*, vol. 66, no. 1, pp. 51-83 (1978); doi: 10.1109/PROC.1978.10837

[5] K. Iizuka, A. P. Freundorfer, K. H. Wu, H. Mori, H. Ogura, and V.-K. Nguyen, Step-frequency radar, *Journal of Applied Physics*, vol. 56, no. 9, pp. 2572-2583 (1984); doi: 10.1063/1.334286

[6] E. Filho, M. Baiad, M. Gagné, and R. Kashyap, Fiber Bragg gratings for low-temperature measurement, Opt. Express 22, 27681-27694 (2014); doi: 10.1364/OE.22.027681

[7] S. Werzinger, S. Bergdolt, R. Engelbrecht, T. Thiel, and B. Schmauss, Quasi-Distributed Fiber Bragg Grating Sensing Using Stepped Incoherent Optical Frequency Domain Reflectometry, in *Journal of Lightwave Technology*, vol. 34, no. 22, pp. 5270-5277 (2016); doi: 10.1109/JLT.2016.2614581

[8] S. Werzinger, M. Gottinger, S. Gussner, S. Bergdolt, R. Engelbrecht, and B. Schmauss, Model-based compressed sensing of fiber Bragg grating arrays in the frequency domain - to be published, in *Proceedings of the International Conference on Optical Fiber Sensors (OFS)*, Jeju, Korea (2017).

[9] R. Engelbrecht, Nichtlineare Faseroptik, *Springer Berlin Heidelberg* (2014). ISBN: 978-3-642-40967-7; doi: 10.1007/978-3-642-40968-4

[10] J. P. Dakin, D. J. Pratt, G. W. Bibby, and J. N. Ross, Distributed optical fibre Raman temperature sensor using a semiconductor light source and detector, in *Electronics Letters*, vol. 21, no. 13, pp. 569-570 (1985); doi: 10.1049/el:1985040